A Statistical Shape Model without Using Landmarks

[1,3]F.M. Vos [2]P.W. de Bruin [1]J.G.M. Aubel [4]G.J. Streekstra [3]M. Maas [1]L.J. van Vliet [1]A.M. Vossepoel

[1] Pattern Recognition Group [2] CG & CAD-CAM Group
[1] Delft University of Technology
Lorentzweg 1
2628 CJ, Delft, The Netherlands

[3] Department of Radiology [4] Department of Medical Physics
Academic Medical Centre
Meibergdreef 1
1105 AZ Amsterdam, The Netherlands

E-mail: frans@ph.tn.tudelft.nl

Abstract

This paper describes the construction of a statistical shape model based on the iterative closest point algorithm. The method does not require manual nor automatic identification of explicit landmarks on example shapes. Corresponding features are found by retrieving the nearest points via interpolation along the surface. The application to analyse carpal bone shape renders evidence that the lunate bone occurs in distinct types.

1. Introduction

Statistical shape models have proven to be useful tools to study variation in anatomical shapes. A popular method captures shape by a sampled 3D point distribution model (PDM) [1]. These models are often created by manually indicating characteristic points on example shapes. However, indicating features by hand is tedious and prone to error. Moreover, many objects have only a few landmarks or have features that are not easily identifiable.

The carpal bones serve as a good example (see Figure 1). Physicians are interested in the shape of carpal bones, because a relation is expected to exist between bone shape and pathological wrist kinematics. Although the shape of each carpal bone is highly characteristic, it is not easy to identify characteristic points.

Preliminary medical studies report on shape features of the carpals in conventional X-ray images [2][3]. The results indicate that there may be distinct types of the lunate bone. Although it confirms observations from clinical practice, the analysis is limited due to the projective nature of the X-ray images.

Recently, several papers describe methods to analyze such shapes via 3D statistical shape models (see e.g. [1][4][5][6][7]). Although the outcomes are very promising, there is not yet a generally accepted framework.

The objective of this work is to construct a non-landmark based statistical shape model. Inspired by [4], an alternative way to find correspondences on multiple shapes is proposed (see 2.2). The method is applicable to any problem in which explicit shape features are not easily identifiable. The novelty is the adaptation of an iterative closest point algorithm and the application to analyse carpal bone shape.

Figure 1. X-ray image showing the left hand wrist in dorsal view. The carpal bones constitute the joint between the metacarpals and the ulna and radius.

2. Methods

We initially follow the procedure first described by Cootes and Taylor [1]. Shape vectors $\boldsymbol{x}_i$ are constructed of n characteristic points in each training image i. Thus, a d-dimensional image results in an nd-element shape vector. Translation, rotation and scale invariance is imposed by aligning the centers of gravity and minimizing the Euclidean distance between the shape vectors under rotation and scaling (Procrustes analysis).

0-7695-2128-2/04 $20.00 (C) 2004 IEEE

The main shape variations are found by principal component analysis, under the assumption of Gaussian distributed data:

1. The mean vector $\bar{\mathbf{x}}$ and covariance matrix $\mathbf{X}$ are calculated by

$$\bar{\boldsymbol{x}} = \frac{1}{m}\sum_{i=1}^{m} \boldsymbol{x}_i \qquad \boldsymbol{X} = \frac{1}{m-1}\sum_{i=1}^{m} (\boldsymbol{x}_i - \bar{\boldsymbol{x}})(\boldsymbol{x}_i - \bar{\boldsymbol{x}})^T \quad (1)$$

in which m indicates the number of training shapes.

2. The eigenvectors ϕ_i and corresponding eigenvalues λ_i are computed and sorted so that $\lambda_i \geq \lambda_{i+1}$.

Let $\Phi = (\phi_1, \phi_2, ..., \phi_k)$ be the matrix of eigenvectors corresponding to the k largest eigenvalues (e.g. summing to 95% of total variance). Shape ($\boldsymbol{x}$) is modelled by:

$$\boldsymbol{x} = \bar{\boldsymbol{x}} + \Phi \boldsymbol{b} \quad (2)$$

in which $\boldsymbol{b} = (b_1, b_2, ..., b_k)$ is a vector containing the shape parameters. Clearly, $\boldsymbol{b} = \mathbf{0}$ yields the average shape. The shape variation along axis i is generated by varying b_i. Suitable limits are: $|b_i| \leq \pm 2\sqrt{\lambda_i} (= 2\sqrt{\sigma_i})$ (σ_i indicates the variance along axis i).

At the basis of the analysis are corresponding points. A technique to find correspondences on two point sets is introduced next (2.1). How to convey this method to a whole set of samples is described in (2.2).

2.1 Correspondence method

The iterative closest point (ICP) algorithm maps one point set (A) onto another (B) [8][4] as follows:

1. Find the closest points to A on B: B'

2. Find the closest points to B on A: A'

3. Find the transformation Q that matches A with B' and B with A'

4. Transform all points via Q

5. Loop until converged

The transformation Q of a point $\mathbf{p}$ is defined by $Q(\mathbf{p}) = sR\mathbf{p} + \mathbf{t}$, in which s is a scale factor (scalar), R is a rotation matrix and $\mathbf{t}$ is a translation vector. An initial estimate for Q is obtained by registering the centers of gravity of the pointsets, aligning the first order moment vectors and equalizing the average distance of the points to the center.

The best match is found in step 3) by minimizing a symmetric distance measure on the point sets:

$$E^2 = \frac{1}{n_A}\sum_{i=1}^{n_A} \left|Q(A) - Q^{-1}(B')\right|^2 + \frac{1}{n_B}\sum_{i=1}^{n_B} \left|Q(A') - Q^{-1}(B)\right|^2 \quad (3)$$

Notice that the shapes are transformed into an intermediate frame, rather than transforming one shape onto the other. This way, preferential treatment of one of the shapes is avoided.

At last, points are mapped from one set on the other by finding the closest points.

2.2 Model construction

The previous method needs to be adjusted to find corresponding points in a whole set of examples. We assume the existence of segmented sample shapes represented by triangle meshes. An accurate surface representation is asserted, but the vertices may not correspond with landmarks. Additionally, mesh size and topology may vary. The meshes are to be "resampled" on corresponding positions to perform shape analysis (2, introduction). We implemented an iterative procedure based on the closest point algorithm (2.1) to do so.

Initially, the mesh with the largest number of vertices ($n_{\max}$) is selected (the pivot mesh). Next, the other meshes are matched to the selected one. At that stage all meshes are resampled to have the same number of corresponding points ($n_{\max}$). Also, the resampled meshes inherit the topology of the pivot mesh. The mean shape is computed by averaging the resampled vertex positions and the whole procedure is repeated by matching the original meshes to this average shape. Thus, a preferential treatment of the mesh with the most vertices is avoided.

One should notice that the Procrustes analysis is embedded in the correspondence method (via Q). Consequently, systematic errors due to an initial misallignment are avoided.

3. Results

All 3D-CT images of the wrist over a period of exactly two years were collected from the Academic Medical Center Amsterdam. This resulted in wrist images from 134

patients, containing 103 right wrists and 107 left wrists. From this set only those wrists were included that did not show signs of pathology according to a radiologist. Among the exclusion criteria were: fractures, arthritis, presence of bone fragments, and bone fusions.

Our focus was on the shape of the lunate and capitate bones since these are typically involved in pathologic wrist kinematics. Unfortunately, the entire wrist was not contained in each scan. Applying the exclusion criteria and considering only completely scanned carpal bones left us with 41 examples of the left lunate, 31 right lunates, 36 left capitate bones and 25 right capitates.

3.1 Model construction

A specially developed software tool [9] was employed to segment the sample shapes from the images. The output of the tool was a triangulated surface description. Both picking the closest points (point-to-point) and interpolating to the nearest position on the triangles (point-to-surface) were considered to find the correspondences (2.1).

Figure 2 illustrates the effect of both approaches on the cumulative relative variance for the left lunate bone (the other carpals had similar outcome). For instance, 80% of the total variance is explained by 23 eigenmodes using point-to-point correspondence and by only 10 eigenmodes via the point-to-surface method.

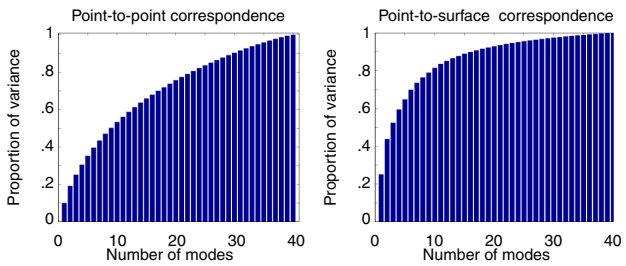

Figure 2. Cumulative relative variance of the left lunate.

The flat profile indicates that the shape analysis via a point-to-point correspondence is hampered by noise (Figure 2, left). This must be due to the irregular positioning of the vertices. The point-to-surface graph signifies an improvement on correspondence. Consequently, true shape description dominates over position errors (Figure 2, right). This is confirmed by the smaller mean distance between corresponding points over all shapes (mean E^2, c.f. Equation 3, see Table 1). Our further analysis employs point-to-surface correspondence.

The stability of the eigenvectors was assessed by their orientation and size as the sample size increased. The first 10, 20 and 30 shapes were selected from the complete set

Table 1: Mean distance between corresponding points

Correspondence method	Mean E^2 (mm)
Point-point	1.9
Point-surface	0.9

of (41) left lunate bones. Table 2 shows the angles between the 4 largest eigenvectors calculated from the subsets and the ones determined from the full set. The table illustrates that the two largest eigenvectors tend to stablize with 30 samples. Higher order eigenvectors seem not to correspond which is indicated by the angles that approximate 0.5 π radians.

Table 2: Angle between eigenvectors from smaller subsets and full set of samples (radians)

#sample shapes	eigenvector			
	1	2	3	4
10	.72	.68	1.2	1.6
20	.35	.38	1.6	1.8
30	.27	.28	.53	2.1

Figure 3 illustrates the effect of sample size on the cumulative relative variance.

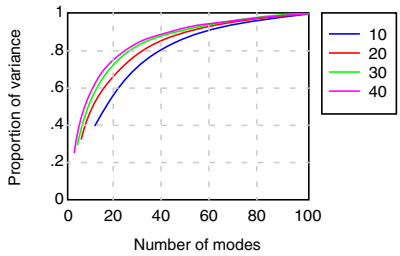

Figure 3. Cumulative relative variance for 10, 20, 30 and the full set of samples.

From Table 2 and Figure 3 we concluded that the point - surface method yields proper estimates of the first 2 eigenvectors.

3.2 Analysis

Earlier work indicates that the lunate bone appears in distinct types, implying multimodally distributed data. Our shape analysis, however, assumes Gaussian distributed data. The validity of this assumption was assessed by the projections of each lunate shape ($\boldsymbol{x}_i$) on the first eigenvector ϕ_1: Figure 4.

Clearly, the right lunate yields a bimodal distribution which confirms the existence of distinct shapes. Accord-

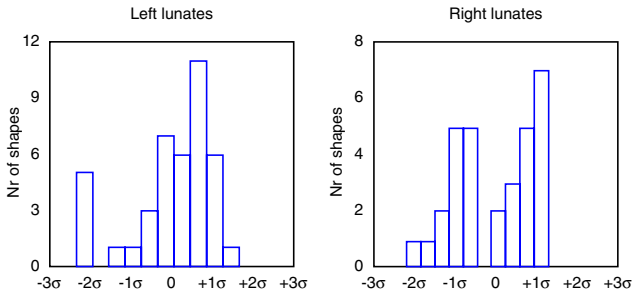

Figure 4. Histograms of lunate shapes projected on the first eigenvector.

ingly, our further analysis considered the two lunate types separately. The left lunate histogram does not justify the distinction. One might attribute this to small sample size. The outliers correspond to bones that have sharp protrusions. The other eigenmodes and the other bones did not deviate significantly from a Gaussian distribution.

The mean right carpal shapes (Figure 5) are realistic

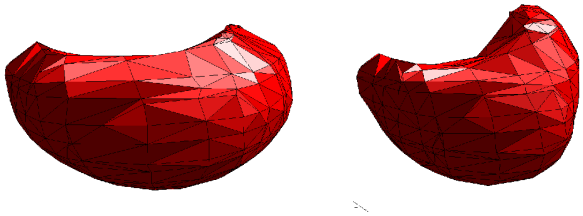

Figure 5. Two distinct right lunate shapes.

representations that agree with how the bones are perceived by clinicians. The left drawing corresponds to the left group in the histogram of Figure 4, the right shape with the right group. The two types of the lunate bone conform to the description of type I and type II lunates [2][3].

The relation between different shapes was explored by way of the shape parameters ($\boldsymbol{b}$, c.f. Equation (2)). The graphs in Figure 6 plot $|\boldsymbol{b}|$ for the left versus the right lunate

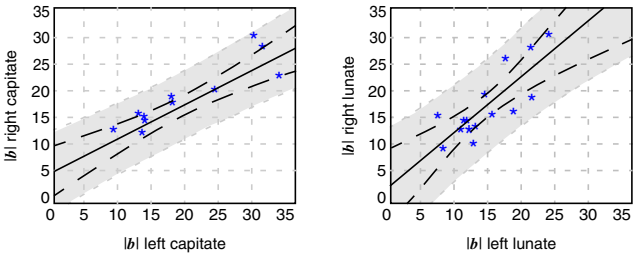

Figure 6. Comparison of carpal shapes in left and right wrist.

and capitate bones, respectively. The shaded area is the 95% prediction interval for the data computed from linear regression. The dashed lines represent the 95% confidence interval for the solid red regression line. Both graphs indicate that a deviation from the average shape in one hand correlates with a deviation in the other. Other relations (e.g. left lunate vs. left capitate, left lunate vs. age etc.) did not yield significant correlations.

4. Conclusion

We described a statistical shape model using an iterative closest point algorithm. The algorithm does not require manual identification of landmarks. A correspondence of features was established by retrieving nearest points on surfaces via interpolation. Such correspondence facilitated the construction of a precise shape model. The shape analysis of the carpal bones rendered further evidence that there are distinct lunate bone shapes. However, a final proof will require more example shapes. For further research, it would be interesting to correlate bone shape with left or right hand dominance as well as pathological kinematics.

We conclude that the method provides a powerful tool, for statistical shape analysis in the absence of natural landmarks.

5. References

[1] T.F. Cootes, C.J. Taylor, D. Cooper, and J. Graham. "Active Shape Models - their training and application", *Computer Vision Image Understanding*, 61(1): 38-59, 1995.

[2] A.H. Schuurman, M. Maas, P.F. Dijkstra, J.M.G. Kauer, "Ulnar variance and the shape of the lunate bone, a radiological investigation", *Acta Orthopaedica Belgica*, 67(5): 464-467, 2001.

[3] J. Taleisnik, *The wrist*, Churchill Livingstone, 1985.

[4] .A.D. Brett, C.J. Taylor, "A method of automated landmark generation for automated 3D PDM construction", *Proc British Machine Vision Conf. 1998*, 914-923.

[5] M. Fleute, S. Lavalee, "Nonrigid 3-D/2-D registration of images using statistical models", *Proc. MICCAI 1999*, vol. 1679 LNCS, Springer-Verlag, 714-721.

[6] R.H. Davies, C.J. Twining, T.F. Cootes, J.C. Waterton, C.J. Taylor, "A minimum description length approach to statistical shape modelling", *IEEE Trans. MI*, 21(5): 525-537, 2002.

[7] D. Rueckert, A.F. Frangi, J.A. Schnabel, "Automatic construction of 3-D Statistical deformation models of the brain using non-rigid registration", *IEEE Trans. MI*, 22(8): 1014-1024, 2003.

[8] P.J. Besl, N.D. McKay, "A method for registration of 3D shapes", *IEEE Trans. on PAMI*, 14(2): 239-256, 1992.

[9] P.W. de Bruin, V.J. Dercksen, F.H. Post, A.M. Vossepoel, G.J. Streekstra, F.M. Vos, "Interactive 3D segmentation using connected orthogonal contours", accepted by Comp.Biol.Med., 2003.